

# Soft Matter

Accepted Manuscript



This is an *Accepted Manuscript*, which has been through the Royal Society of Chemistry peer review process and has been accepted for publication.

*Accepted Manuscripts* are published online shortly after acceptance, before technical editing, formatting and proof reading. Using this free service, authors can make their results available to the community, in citable form, before we publish the edited article. We will replace this *Accepted Manuscript* with the edited and formatted *Advance Article* as soon as it is available.

You can find more information about *Accepted Manuscripts* in the [Information for Authors](#).

Please note that technical editing may introduce minor changes to the text and/or graphics, which may alter content. The journal's standard [Terms & Conditions](#) and the [Ethical guidelines](#) still apply. In no event shall the Royal Society of Chemistry be held responsible for any errors or omissions in this *Accepted Manuscript* or any consequences arising from the use of any information it contains.

Cite this: DOI: 10.1039/xxxxxxxxxx

## Dynamic moduli of magneto-sensitive elastomers: a coarse-grained network model

Dmytro Ivaneyko,<sup>\*a</sup> Vladimir P. Toshchevnikov,<sup>a,b</sup> and Marina Saphiannikova<sup>a</sup>Received Date  
Accepted Date

DOI: 10.1039/xxxxxxxxxx

www.rsc.org/journalname

The viscoelastic properties of magneto-sensitive elastomers (MSEs) in a low-frequency regime are studied using a coarse-grained network model. The proposed model takes into account the mechanical coupling between magnetic particles included in a whole network structure and magnetic interactions between them. We show that the application of a constant uniform magnetic field leads to the splitting of the relaxation spectrum into two branches for the motions of the particles parallel and perpendicular to the field. The shear dynamic moduli  $G'$  and  $G''$  of MSEs are calculated as functions of frequency. The values of  $G'$  and  $G''$  are shown to depend on the direction of the shear deformation with respect to the magnetic field. For instance, both  $G'$  and  $G''$  decrease if the magnetic field is applied parallel to the shear velocity (**D**-geometry) and increase if it is applied along the shear gradient (**G**-geometry). The latter prediction is in a qualitative agreement with existing experimental data. The theory allows to analyse experimental data and to extract the structural characteristics of MSEs.

### 1 Introduction

Two-component polymer composites, consisting of a soft non-magnetic polymer network and magnetic filler particles, are smart materials, which can change their mechanical properties under application of the external magnetic field. Such materials are often called magneto-sensitive elastomers (MSEs), magnetorheological elastomers (MREs) or, sometimes, soft magnetic elastomers (SMEs).<sup>1</sup> Under external magnetic field, MSEs acquire peculiar properties: they change their elasticity (the shear and Young's moduli) and shape. Due to such smart behaviour, MSEs are widely used nowadays in many technical applications: controllable membranes, rapid-response interfaces designed to optimize mechanical systems and in automobile applications such as adaptive tuned vibration absorbers, stiffness tunable mounts and automobile suspensions.<sup>2,3</sup>

Different kinds of magnetizable particles with different shapes and sizes can be used as magnetic fillers. However, the particles prepared from carbonyl iron with the size from hundreds nanometers to several micrometers are mostly used due to their high magnetic permeability.<sup>4-6</sup> Although the microsize carbonyl iron particles have a multi-domain magnetic structure, very narrow hysteresis cycles for the powders and composites with these particles were observed which indicate a soft magnetic be-

haviour.<sup>4-6</sup> Such particles have shape close to an ideal sphere that simplifies dispersion of the particles within a polymer melt before its cross-linking. Besides, the carbonyl iron particles in a polymer melt are not magnetized and do not create inhomogeneities like clusters or agglomerates in the absence of the external magnetic field. Therefore, one can synthesize the MSEs with perfect isotropic particle distribution.<sup>4,6,7</sup> Moreover, the anisotropic chain-like or plane-like particle distribution can be produced by means of application of the magnetic field before the cross-linking of a polymer melt.<sup>4,6,8</sup>

Due to high importance of MSEs for practice, their mechanical properties have been extensively studied during the last decade. There are a lot of experimental works,<sup>9-12</sup> theoretical studies<sup>13-20</sup> and computer simulations<sup>1,21,22</sup> devoted to mechanical properties of MSEs in the equilibrium (static) state. Static magneto-induced deformation, as well as the change of the static Young's modulus and static shear modulus under external magnetic field have been investigated. On the other hand, very important topic is the dynamic-mechanical behaviour of MSEs, since in various technical applications these materials can be influenced by the oscillating mechanical loading.<sup>3,23,24</sup> There are a lot of experimental works which discuss the influence of the external constant magnetic field on the frequency dependences of the storage  $G'$  and loss  $G''$  moduli.<sup>6,25-30</sup> It was shown that the values of  $G'$  and  $G''$  at a given frequency  $f$  depend on the magnitude of the external magnetic field. For the shear geometry with the shear velocity perpendicular to the magnetic field vector **H** (**G**-geometry in Fig. 1) both  $G'$  and  $G''$  are found to increase with

<sup>a</sup> Leibniz-Institut für Polymerforschung Dresden, Germany. Fax: +49(0)351 4658 752; Tel: +49(0)351 4658 657; E-mail: ivaneiko@ipfdd.de

<sup>b</sup> Institute of Macromolecular Compounds, Russian Academy of Science, Saint-Petersburg, Russia

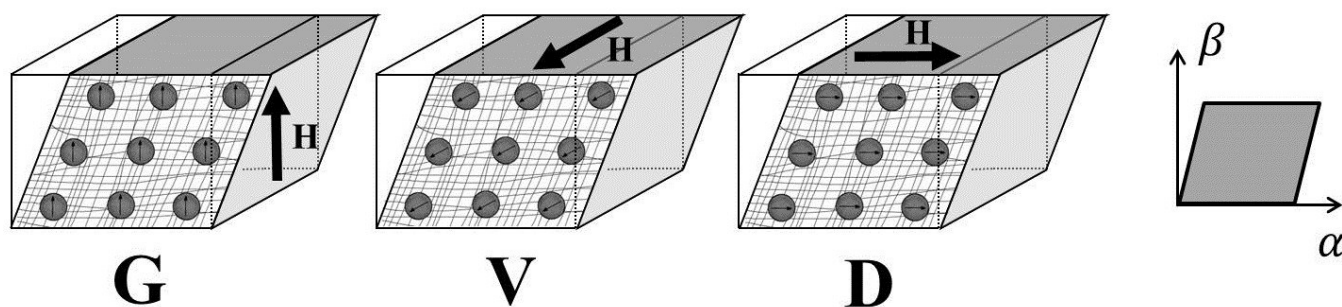


**Fig. 1** Three principal geometries of the shear deformation with respect to the direction of the magnetic field vector  $\mathbf{H}$ : shear gradient geometry **G**, vorticity geometry **V** and displacement geometry **D**. Shear deformation is applied along the  $\alpha$ -axis and the shear gradient is along the  $\beta$ -axis.

the increase of the magnitude of external magnetic field at fixed frequency. Influence of structural parameters, such as the volume fraction of the magnetic particles and the degree of cross-linking of an elastomeric matrix, on the dynamic mechanical behaviour of MSEs under magnetic field has been discussed in a number of experimental works.<sup>25–27,29</sup>

Although the experimental study of the dynamic-mechanical properties of MSEs has been performed extensively, the structure-property relationships for dynamic behaviour of MSEs are understood not so well from theoretical point of view. The frequency dependences of the storage and loss moduli of MSEs have been analysed using some phenomenological approaches.<sup>31–33</sup> However, these works do not discuss the relationship between the microstructure of MSEs and phenomenological parameters included into the theories. The relaxation spectrum of ferrogels was recently studied, using a microscopic 1D and 2D dipole-spring models.<sup>34</sup> However, the dynamic moduli were not considered in the literature using microscopic models. Moreover, MSEs under magnetic field become anisotropic and, thus, should demonstrate anisotropy of their dynamic-mechanical behaviour. One can expect that the dynamic moduli should depend on the geometry of the shear application with respect to the magnetic field (see Fig. 1), as it was shown, e.g., for anisotropic liquid-crystalline (LC) networks.<sup>35</sup> Note that the anisotropy of the static Young's modulus for MSEs has been considered theoretically.<sup>16</sup> On the other hand, anisotropy of the dynamic moduli of MSEs was not discussed in the literature at all.

In order to overcome these drawbacks, in the present study we propose a coarse-grained dynamic model, which allows to study the dynamic-mechanical properties of MSEs in a low-frequency regime depending on the MSE microstructure. The model takes explicitly into account the effects of interactions between magnetic particles on the dynamics of MSEs. Using this model, the frequency dependences of the storage and loss moduli of MSEs for the **G**-, **V**- and **D**-geometries are calculated as functions of the strength of the magnetic field depending on the volume fraction of magnetic particles, their magnetization and the elasticity of polymer matrix, which is related to the degree of cross-linking. The obtained structure-property relationships are in agreement with experiments and can be of a high importance for practical applications.

## 2 Dynamic model of MSE and its validity range

To begin with, it should be emphasized that theoretical description of dynamic behaviour of real polymer networks is a complex task even for isotropic polymers, because the dynamic properties depend strongly on the structure of the networks. This results in a complex character of network relaxation. Different effects on the dynamics have been discussed in literature such as: incorporation of polymer chains into a united network structure,<sup>36–38</sup> heterogeneous distribution of cross-links,<sup>38,39</sup> polydispersity of network strands,<sup>38,40</sup> the presence of dangling chains and loops,<sup>41–43</sup> possible fractal structures of network domains,<sup>38,44,45</sup> etc. These works demonstrate clearly that the frequency dependences of the dynamic moduli are very sensitive to the structure of polymer networks, for more details see the review.<sup>38</sup> Thus, for each particular kind of network structure one needs a special network model.

On the other hand, the cubic network model is widely used to describe the mechanical properties of three-dimensional isotropic polymer networks.<sup>35–39,46–49</sup> In ref.<sup>48</sup> it was shown that the mechanical properties under external stress, provided by cubic network model, coincide with the results for Gaussian networks with random orientations of the network strands in the linear response regime. The prediction of the cubic network model for the storage modulus,  $G' - G^{(eq)} \propto \omega^{3/2}$ , is fulfilled for synthesized networks, e.g. for poly[oxi(methylsilylene)]'s networks, see ref.<sup>35</sup> Such low-frequency scaling behavior of the storage modulus around the low-frequency plateau,  $G^{(eq)}$ , corresponds to a collective motion of chains incorporated into a united network structure.<sup>35–38</sup> Thus, the cubic network model takes explicitly into account the three-dimensional connectivity of chains in a polymer network. Moreover, the cubic network model describes quite well the dynamics of heterogeneous elastomeric matrices with domain structure.<sup>38,39</sup>

The aim of our work is to study the effect of magnetic field on the moduli of MSEs. We are interested in the change of the moduli under application of magnetic field as compared to the moduli for the reference system, i.e. for the network at absence of the magnetic field. Since the cubic network model was widely used to describe the dynamics of polymer networks, we start from the cubic network as a reference system to study the dynamics of

MSEs.

The present study focuses on the low-frequency viscoelastic behaviour of MSEs with isotropic distribution of magnetic particles (see Fig. 2a) at scales longer than the distance between neighbouring particles. In this regime the relaxation processes inside each network domain which contains one magnetic particle are finished and the dynamics of the network domains between neighbouring particles can be described by simple Hookean springs. Furthermore, it is assumed that the isotropically distributed magnetic particles fluctuate around their average positions on the sites of the cubic lattice. Thus, to describe the dynamics of MSEs in the long-scale regime we use a coarse-grained cubic network model, its cell is shown on Fig. 2b. The length of the edge,  $a$ , equals the average distance between neighbouring particles and is related to the volume fraction of the particles,  $\phi$ :

$$\phi = \frac{v}{a^3}, \quad (1)$$

where  $v$  is the volume of one magnetic particle.

The mobility of particles in the model is determined by the elasticity constant  $K$  of the Hookean spring and by the friction coefficient  $\zeta$  of the network junction. The friction coefficient  $\zeta$  in the coarse-grained model describes the dissipative effects which appear under displacement of the neighbouring magnetic particles on the long scales. The elasticity constant  $K$  describes entropic losses in network domains under displacement of the neighbouring particles with respect to each other. The value  $K$  can be related to the static modulus of an MSE at the absence of the magnetic field using the following argument. Application of the shear strain  $\gamma$  along the  $y$ -axis, for example, results in the appearance of the mechanical force,  $F$ , acting on a given particle due to deformation of the spring:  $F = K\Delta y$ , where  $\Delta y = \gamma a$ . Thus, the mechanical stress is equal to  $\sigma = F/a^2 = K\gamma/a$  and the shear modulus  $G_0 = \sigma/\gamma$  is given by:

$$G_0 = K/a. \quad (2)$$

For isotropic incompressible media the shear modulus is three times smaller than the tensile Young's modulus  $E_0$ :  $G_0 = E_0/3$ . Typical values of the shear modulus for MSEs are from 10 kPa to 100 kPa.<sup>25–27,29,50,51</sup>

Note, that the introduced coarse-grained network model, proposed originally in ref.<sup>36</sup>, was widely used to describe the long-scale dynamics of usual non-magnetic rubbers. It allowed to study the collective motions of network fragments included into a whole network structure. In refs.<sup>37,38,47</sup> it was shown that the coarse-grained network model describes correctly the low-frequency dynamics of multi-segmental network models. Recently, the coarse-grained network model was modified to study the low-frequency dynamics of polymer networks with included particles<sup>46,49</sup> as well as the dynamics of anisotropic networks with LC-order<sup>35</sup> or under external forces.<sup>48,52</sup> As in the previous works for networks of different structure,<sup>35–38,46–49,52</sup> we start from the coarse-grained cubic network model in order to study the low-scale dynamics of magneto-sensitive elastomers. Using this model, we take explicitly into account both the elastic interactions between the magnetic particles included into a united

network structure and the magnetic interactions between them.

Application of a constant magnetic field of the magnitude  $H$  induces an average magnetic moment  $m = Mv$  in each particle along the direction of the field. Here  $M$  is the magnetization of the particles which is a function of the magnetic field  $H$ . The dependence  $M(H)$  can be estimated using other theoretical works.<sup>15,53</sup> The magnetic field  $\mathbf{H}$  is assumed to be directed along the  $x$ -axis (see Fig. 2b).

The dipole-dipole interactions between the magnetic particles influence the molecular mobility of an MSE. The mobility of a given particle is determined by the potential,  $U(\mathbf{r}_n)$ , acting on this particle from other ones. This potential includes the mechanical and magnetic parts:

$$U(\mathbf{r}_n) = U_{mech}(\mathbf{r}_n) + U_{magn}(\mathbf{r}_n), \quad (3)$$

where  $\mathbf{r}_n$  is the position vector of the  $n$ -th particle. Here we introduced the 3D index  $\mathbf{n} = (n_x, n_y, n_z)$ , which numerates the particles in the cubic network model (see Fig. 2b). The components  $n_x$ ,  $n_y$  and  $n_z$  count the particles in the  $x$ -,  $y$ - and  $z$ -directions and run over all integer values:  $n_{x,y,z} = \dots, -1, 0, +1, \dots$ . The mechanical part in eqn (3) is given by:

$$U_{mech}(\mathbf{r}_n) = \frac{1}{2}K \sum_{\mathbf{n}'} C_{\mathbf{n}\mathbf{n}'} (\mathbf{r}_n - \mathbf{r}_{\mathbf{n}'})^2, \quad (4)$$

where the coefficient  $C_{\mathbf{n}\mathbf{n}'} = 1$  if the  $\mathbf{n}$ - and  $\mathbf{n}'$ -th particles are connected by the spring and  $C_{\mathbf{n}\mathbf{n}'} = 0$  otherwise. The magnetic part has the following form for induced magnetic moments in the linear response regime:<sup>54</sup>

$$U_{magn}(\mathbf{r}_n) = -\frac{\mu_0}{8\pi} v^2 M^2 \sum_{\mathbf{n}'} \frac{3(x_{\mathbf{n}'} - x_n)^2 - (\mathbf{r}_{\mathbf{n}'} - \mathbf{r}_n)^2}{|\mathbf{r}_{\mathbf{n}'} - \mathbf{r}_n|^5}, \quad (5)$$

where  $\mu_0$  is the permeability of the vacuum.

The last equation uses the approximation of point-like dipole-dipole interactions between magnetic particles. It was shown in ref.<sup>54</sup> that this approximation describes very well the interactions of magnetic particles of a finite radius  $r$  at separation distances  $a > 3r$ . The condition  $a > 3r$  corresponds to the volume fractions  $\phi < \phi_c$ , where  $\phi_c$  is defined from the condition that each particle occupies on the average the volume of a sphere with the radius  $1.5r$ :  $\phi_c \sim r^3/(1.5r)^3 \sim 30\%$ . Note, the typical MSEs have concentration of the particles that usually does not exceed 30–35%.<sup>26,29,55</sup> Thus, the approximation of point-like interactions of magnetic particles given by eqn (5) is quite reasonable to analyze the dynamics of MSEs with isotropic particle distribution.

The validity range of the introduced model is determined by a condition of the stable equilibrium for the position of particles on the sites of the cubic lattice. The stable equilibrium means that the positions of particles on the sites of the cubic lattice correspond to minima of the energy  $U(\mathbf{r}_n)$ . To estimate the validity range of the model, let's consider a small displacement of an  $n$ -th particle,  $\delta\mathbf{r}_n$ , from its average position taking into account the influence of the nearest neighbours with the numbers  $(n_x \pm 1, n_y, n_z)$ ,  $(n_x, n_y \pm 1, n_z)$  and  $(n_x, n_y, n_z \pm 1)$ . Positions of the neighbouring particles are assumed to be fixed. As it follows from eqn (4), the mechanical potential  $U_{mech}(\delta\mathbf{r}_n)$  has a local minimum for motions

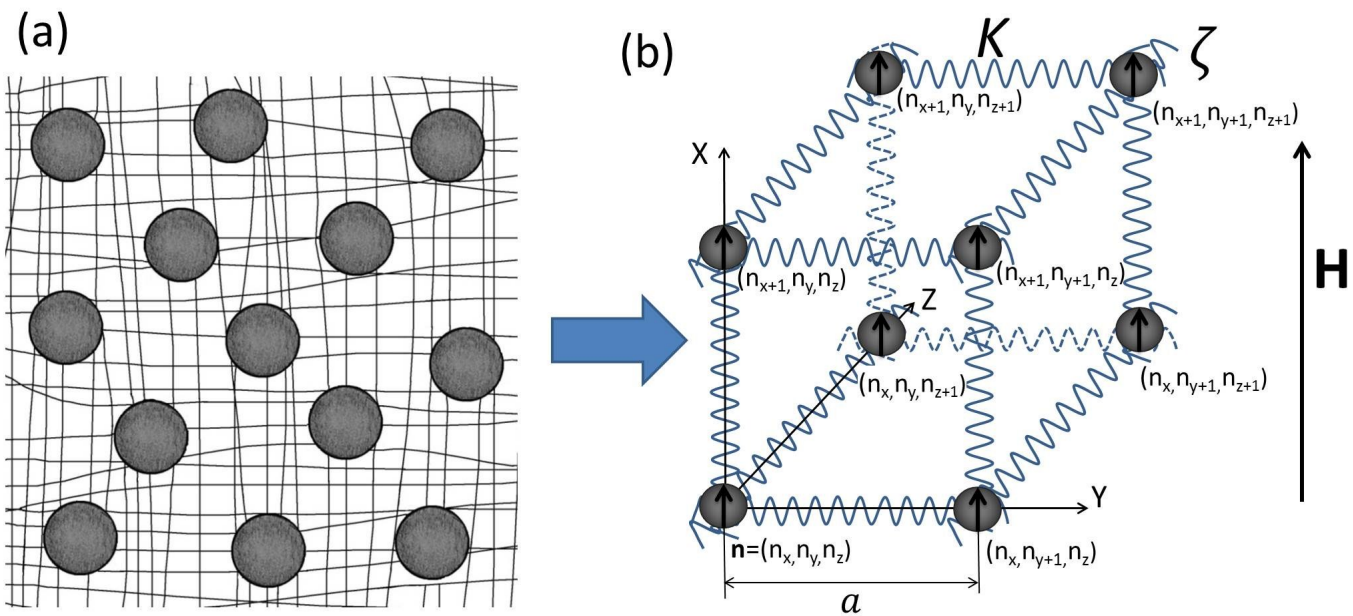


**Fig. 2** Schematic representation of an MSE with magnetic particles, isotropically distributed inside an elastomer matrix (a). The cell of the coarse-grained cubic network model, see text for details (b).

in all directions:  $U_{mech}(\delta \mathbf{r}_n) = 3K(\delta x_n^2 + \delta y_n^2 + \delta z_n^2)$ . However, the change of the magnetic potential depends on the direction of the displacement. Using eqn (5), we find that for the motion perpendicular to the magnetic field ( $\delta y_n \neq 0, \delta x_n = \delta z_n = 0$ ) the change of the magnetic potential is positive:

$$U_{magn}(\delta y_n) = \frac{21\mu_0}{8\pi} \frac{v^2 M^2}{a^5} \delta y_n^2. \quad (6)$$

On the other hand, using eqn (5), we find that for the motion parallel to the magnetic field ( $\delta x_n \neq 0, \delta y_n = \delta z_n = 0$ ) the change of the magnetic potential is negative:

$$U_{magn}(\delta x_n) = -\frac{21\mu_0}{4\pi} \frac{v^2 M^2}{a^5} \delta x_n^2. \quad (7)$$

Thus, for the motion perpendicular to the magnetic field the total potential has a local minimum at any values of  $M$ :

$$U(\delta y_n) = \left(3K + \frac{21\mu_0}{8\pi} \frac{v^2 M^2}{a^5}\right) \delta y_n^2 = 3K \left(1 + \frac{1}{2} \left(\frac{M}{M^*}\right)^2\right) \delta y_n^2, \quad (8)$$

whereas for the motion parallel to the magnetic field the change of the potential  $U(\delta x_n)$  is determined by an interplay between the mechanical and magnetic parts:

$$U(\delta x_n) = 3K \left(1 - \frac{7\mu_0}{4\pi} \frac{v^2 M^2}{Ka^5}\right) \delta x_n^2 = 3K \left(1 - \left(\frac{M}{M^*}\right)^2\right) \delta x_n^2. \quad (9)$$

Here we have introduced a critical value of the magnetization  $M^*$ , which can be written in the following form using eqn (1) and (2):

$$M^* = \left(\frac{4\pi G_0}{7\mu_0 \phi^2}\right)^{1/2} = \left(\frac{4\pi E_0}{21\mu_0 \phi^2}\right)^{1/2}. \quad (10)$$

One can see that at  $M < M^*$  the potential energy  $U(\delta \mathbf{r}_n)$  has a local minimum at  $\delta \mathbf{r}_n = 0$ , whereas at  $M > M^*$  it is characterized by a saddle point at  $\delta \mathbf{r}_n = 0$ . Thus, at  $M > M^*$  an unstable equilibrium state takes place at  $\delta \mathbf{r}_n = 0$  and the particles are expected to rearrange and to form chain-like agglomerates along the magnetic field. The formation of chain-like agglomerates under magnetic field has been discussed in many experimental works.<sup>6,8,56</sup> At the same time, theoretical description of this effect is not a trivial problem, since (i) the quadratic terms of the mechanical potential  $U_{mech}(\delta \mathbf{r}_n) \sim \delta \mathbf{r}_n^2$  are not enough to compensate the magnetic potential, as can be seen from eqn (9), and the nonlinear elasticity should be taken into account; (ii) irregularity of the local spatial distribution of particles can play a significant role for the rearrangement. Therefore, the rearrangement of the particles is not considered in the present study, which deals exclusively with the dynamics of MSEs with homogeneously distributed particles at  $M < M^*$ .

The critical value  $M^*$  can be related to the critical value of the external magnetic flux density  $B^*$  which determines the boundary between two regimes mentioned above. To estimate  $B^*$  we use the relationship between the magnetic field  $\mathbf{B}$  and the magnetization  $\mathbf{M}$  in the linear response regime. For a spherical particle with a high magnetic susceptibility ( $\chi \gg 1$ ) inside a spherical sample this relationship is given by:  $M = 3B/\mu_0$ .<sup>57</sup> Using the last relationship and eqn (10), the value of  $B^*$  is estimated as:

$$B^* = \left(\frac{4\pi\mu_0 G_0}{63\phi^2}\right)^{1/2} = \left(\frac{4\pi\mu_0 E_0}{189\phi^2}\right)^{1/2}. \quad (11)$$

For sufficiently stiff MSEs (with  $G_0 \sim 100$  kPa) and at  $\phi \sim 0.2$  as in experiment,<sup>25</sup> the value of  $B^*$  is estimated to be  $\sim 790$  mT. Note that the region  $B < 800$  mT is used in this experiment.<sup>25</sup> This illustrates that our model is applicable in a broad region of mag-

netic fields for sufficiently stiff MSEs. For sufficiently soft MSEs ( $E_0 \sim 20$  kPa) and at  $\phi \sim 0.2$  as in experiment,<sup>50</sup> the value  $B^*$  is estimated to be  $\sim 200$  mT. The range  $B < B^*$  for soft MSEs is shorter as compared to more stiff MSEs, but nevertheless it is comparable with the magnetic fields ( $B < 400$  mT) used in experiments. Thus, the proposed dynamic model is applicable to study the dynamic-mechanical properties of MSEs in experimentally investigated region of the magnetic field.

### 3 Equations of motion. Relaxation spectrum

The equation of motion for the position vector  $\mathbf{r}_n$  of the  $n$ -th junction in the coarse-grained network model is given by the Langevin equation:

$$\zeta \dot{\mathbf{r}}_n + \frac{\partial U(\mathbf{r}_n)}{\partial \mathbf{r}_n} = \mathbf{F}_n^{(\text{Br})} + \mathbf{F}_n^{(\text{Ext})}, \quad (12)$$

where  $\dot{\mathbf{r}}_n$  is the time derivative:  $\dot{\mathbf{r}}_n = d\mathbf{r}_n/dt$ ,  $\mathbf{F}_n^{(\text{Br})}$  is the Brownian force and  $\mathbf{F}_n^{(\text{Ext})}$  is the external force acting on the particle

due to oscillating mechanical loading. The potential  $U(\mathbf{r}_n)$  of the  $n$ -th particle in the magnetic field is given by eqn (3) and (5). As it was discussed in many monographs,<sup>58–60</sup> the inertial term can be neglected as compared to the viscous drag term in a good approximation for the viscoelastic polymer materials.

The position vector  $\mathbf{r}_n$  of the magnetic particle can be presented as a sum of its average value,  $\mathbf{r}_n^{(0)}$ , and deviation from this value,  $\delta\mathbf{r}_n$ :

$$\mathbf{r}_n = \mathbf{r}_n^{(0)} + \delta\mathbf{r}_n. \quad (13)$$

One can see from eqn (5) and (12) that the dynamics of an MSE is determined by a non-linear equation of motion when taking into account the magnetic interactions. However, for calculation of the dynamic moduli in the linear response regime we can use linearization of the equation of motion with respect to small deviations  $|\delta\mathbf{r}| \ll a$ . Substituting eqn (3) and (5) into (12) and using this linearization, the equation of motion for  $\delta\mathbf{r}_n$  can be rewritten in the following matrix form:

$$\zeta \delta\dot{\mathbf{r}}_n + K \sum_{n'} C_{nn'} (\delta\mathbf{r}_n - \delta\mathbf{r}_{n'}) + 12K \left( \frac{M}{M^*} \right)^2 \sum_{\mathbf{k}} \hat{a}(\mathbf{k}) (\delta\mathbf{r}_n - \delta\mathbf{r}_{n+\mathbf{k}}) = \mathbf{F}_n^{(\text{Br})} + \mathbf{F}_n^{(\text{Ext})}, \quad (14)$$

where components of the symmetric matrix  $\hat{a}$  are given by:

$$a_{xx}(\mathbf{k}) = \frac{8k_x^4 - 24k_x^2(k_y^2 + k_z^2) + 3(k_y^2 + k_z^2)^2}{56k^9}, \quad (15)$$

$$a_{yx}(\mathbf{k}) = a_{xy}(\mathbf{k}) = \frac{5k_x k_y (4k_x^2 - 3k_y^2 - 3k_z^2)}{56k^9}, \quad (16)$$

$$a_{zx}(\mathbf{k}) = a_{xz}(\mathbf{k}) = \frac{5k_x k_z (4k_x^2 - 3k_y^2 - 3k_z^2)}{56k^9}, \quad (17)$$

$$a_{yy}(\mathbf{k}) = -\frac{4k_x^4 + 4k_y^4 - k_z^4 + 3(k_x^2 + k_y^2)k_z^2 - 27k_x^2 k_y^2}{56k^9}, \quad (18)$$

$$a_{yz}(\mathbf{k}) = a_{zy}(\mathbf{k}) = \frac{5k_y k_z (6k_x^2 - k_y^2 - k_z^2)}{56k^9}, \quad (19)$$

$$a_{zz}(\mathbf{k}) = -\frac{4k_x^4 + 4k_z^4 - k_y^4 + 3(k_x^2 + k_z^2)k_y^2 - 27k_x^2 k_z^2}{56k^9}. \quad (20)$$

In eqn (14) the index  $\mathbf{k} = \mathbf{n}' - \mathbf{n}$  was introduced and the relationship  $\mathbf{r}_{n'}^{(0)} - \mathbf{r}_n^{(0)} = a\mathbf{k}$  was used. Besides, to derive eqn (14), the relation (10) between  $M^*$  and the structural parameters  $\phi$ ,  $v$  and  $E_0$  was taken into account. To solve eqn (14) we use the new coordinates, which for the cubic network are related to the Fourier transform:<sup>35–38,46,47,49,52</sup>

$$\mathbf{Q}(\boldsymbol{\theta}) = \sum_{\mathbf{n}} \delta\mathbf{r}_n e^{i\mathbf{n}\boldsymbol{\theta}}, \quad (21)$$

where  $\mathbf{n}\boldsymbol{\theta}$  is the scalar product of the vectors. The components of the vector  $\boldsymbol{\theta} = (\theta_x, \theta_y, \theta_z)$  change within the range from 0 to  $\pi$ :  $\theta_{x,y,z} \in [0, \pi]$ . Similar to the classical Rouse model,<sup>58</sup> the different values of  $\boldsymbol{\theta}$  determine different scales of motion in the 3D network. For instance, the limiting values of  $\boldsymbol{\theta} \rightarrow (0, 0, 0)$  de-

termine the long-scale dynamic modes with co-phase motion of neighbouring particles. The limiting values of  $\boldsymbol{\theta} \rightarrow (\pi, \pi, \pi)$  determine the short-scale dynamic modes with anti-phase motion of neighbouring particles.<sup>35–38,46,47,49,52</sup>

The solution of the system of eqn (14) relative to the components  $\delta r_x, \delta r_y, \delta r_z$  of the vector  $\delta\mathbf{r}_n$  as a function of external forces  $\mathbf{F}_n^{(\text{Br})}$  and  $\mathbf{F}_n^{(\text{Ext})}$  can be derived from a general solution of a homogeneous system of these equations, whose right sides are equal to zero:  $\mathbf{F}_n^{(\text{Br})} = 0$  and  $\mathbf{F}_n^{(\text{Ext})} = 0$ . The solution of the homogeneous system of equations determines such important characteristics of MSEs as normal modes and the relaxation-time spectrum. Multiplying both parts of eqn (14) by the factor  $e^{i\mathbf{n}\boldsymbol{\theta}}$  and taking a sum over the index  $\mathbf{n}$ , we obtain the homogeneous system of equations in the following matrix form:

$$\hat{\mathbf{Q}}(\boldsymbol{\theta}) + \frac{1}{\tau_0} \hat{\mathbf{B}}\mathbf{Q}(\boldsymbol{\theta}) = 0, \quad (22)$$

where  $\tau_0 = \frac{\zeta}{12K}$  is the minimal relaxation time of the cubic network at the absence of the magnetic field.<sup>37</sup> The matrix  $\hat{\mathbf{B}}$  has the following form:

$$\hat{\mathbf{B}} = \lambda_0 \hat{\mathbf{I}} + \left( \frac{M}{M^*} \right)^2 \hat{\mathbf{A}}, \quad (23)$$

where  $\lambda_0$  is a function of  $\boldsymbol{\theta}$ :  $\lambda_0 = \frac{1}{6} [3 - \cos(\theta_x) - \cos(\theta_y) - \cos(\theta_z)]$ ,  $\hat{\mathbf{I}}$  is the  $3 \times 3$  unit matrix and the matrix  $\hat{\mathbf{A}}$  is related to the symmetrical matrix  $\hat{a}$ :

$$A_{\alpha\beta} = \sum_{\mathbf{k}} a_{\alpha\beta}(\mathbf{k}) (\cos(\mathbf{k}\boldsymbol{\theta}) - 1). \quad (24)$$

Note that the non-diagonal coefficients of the matrix  $\hat{\mathbf{A}}$  are not equal to zero:  $A_{\alpha\beta} \neq 0$  at  $\alpha \neq \beta$  ( $\alpha, \beta = x, y, z$ ). This means that

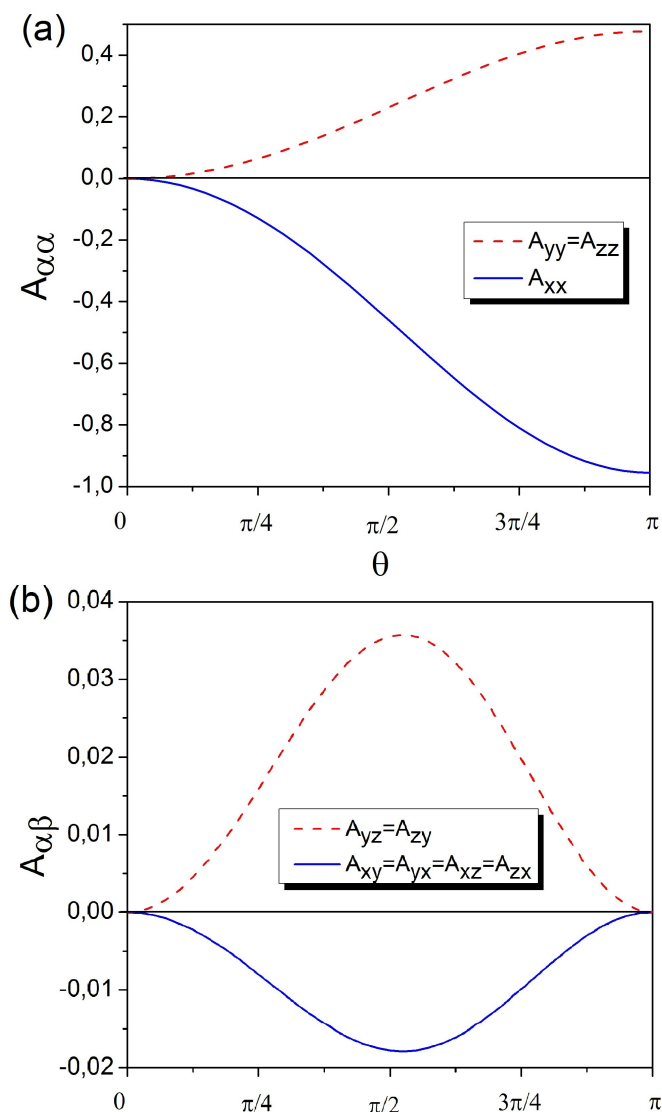


**Fig. 3** Coefficients  $A_{\alpha\beta}$ , where  $\alpha, \beta = x, y, z$  as functions of  $\theta = \theta_x = \theta_y = \theta_z$ .

the dynamics along a given axis depends on the motion along the other axes. However, as we will show below, the contribution of the non-diagonal elements of the matrix  $\hat{A}$  to the dynamic-mechanical characteristics can be neglected in a good approximation.

The sum in eqn (24) is performed over the components of the 3D index  $\mathbf{k}$ , where  $k_\alpha$  change within the range of integer numbers from  $-N$  to  $N$ . As in ref.<sup>17</sup> we have found that the sum over  $\mathbf{k}$  converges already at  $N \approx 10$ . To obtain results with the high accuracy, we calculate the sum over  $\mathbf{k}$  at  $N = 20$ . Fig. 3 shows the coefficients  $A_{\alpha\beta}$  at equal values of the components of the vector  $\boldsymbol{\theta}$  ( $\theta_x = \theta_y = \theta_z \equiv \theta$ ) as a function of the parameter  $\theta$ . Note that according to eqn (15)-(20) and (24)  $A_{yy} = A_{zz}$ ,  $A_{xy} = A_{yx} = A_{xz} = A_{zx}$  and  $A_{yz} = A_{zy}$  at  $\theta_x = \theta_y = \theta_z$ .

One can see from Fig. 3 that absolute values of the non-diagonal coefficients  $A_{\alpha\beta}$  (at  $\alpha \neq \beta$ ) are much smaller than absolute values of the diagonal coefficients  $A_{\alpha\alpha}$  and, thus, can be

neglected at  $\theta_x = \theta_y = \theta_z$ . In a general case with  $\theta_x \neq \theta_y \neq \theta_z$  all elements of the matrix  $\hat{A}$  differ from each other:  $A_{xx} \neq A_{yy} \neq A_{zz} \neq A_{xy} \neq A_{xz} \neq A_{yz}$ . The contribution of non-diagonal elements at  $\theta_x \neq \theta_y \neq \theta_z$  to the solution of eqn (22) is discussed below.

The solution of eqn (22) can be found in the following form:

$$\mathbf{Q} = \mathbf{V}e^{-t/\tau}, \quad (25)$$

where  $\tau$  is the relaxation time for a given normal coordinate. It is convenient to introduce a dimensionless inverse relaxation time  $\lambda = \tau_0/\tau$ . Substituting eqn (25) into (22), we get equation for  $\lambda$  in the following form:

$$\hat{B}\mathbf{V} = \lambda\mathbf{V}. \quad (26)$$

Thus, the vector  $\mathbf{V}$  is the eigenvector of the matrix  $\hat{B}$  and the relaxation time  $\tau$  is related to the eigenvalues  $\lambda$  of the matrix  $\hat{B}$ .

We calculated numerically the three eigenvalues  $\lambda_1 < \lambda_2 < \lambda_3$  of the matrix  $\hat{B}$  as functions of  $\theta_x, \theta_y, \theta_z$ . The results of numerical calculations of  $\lambda_i$  ( $i = 1, 2, 3$ ) were compared with the approximation, in which the non-diagonal elements of matrix  $\hat{A}$  are equal to 0. In this approximation, the eigenvalues of the matrix  $\hat{B}$  can be written in the following simple form:

$$\lambda_\alpha(\boldsymbol{\theta}) = \lambda_0(\boldsymbol{\theta}) + \left(\frac{M}{M^*}\right)^2 A_{\alpha\alpha}(\boldsymbol{\theta}), \quad (27)$$

where  $\alpha = x, y, z$ . One can see that  $\lambda_x, \lambda_y$  and  $\lambda_z$  are functions of the  $\theta_x, \theta_y, \theta_z$  and depend on the parameter  $M/M^*$ . Besides, it can be seen that  $\lambda_y = \lambda_z$  at  $\theta_x = \theta_y = \theta_z$ . Note that  $\lambda_0$  describes the eigenvalues  $\lambda$  for the isotropic cubic network at the absence of any fields.<sup>35,37,38</sup>

Fig. 4 shows the eigenvalues  $\lambda$  at  $\theta_x = \theta_y = \theta_z = \theta$  as functions of  $\theta$  for  $M/M^* = 0.5$  (a) and  $M/M^* = 0.9$  (b). The solid lines with symbols illustrate the result for exact eigenvalues  $\lambda_1, \lambda_2, \lambda_3$  obtained by numerical diagonalization of the matrix  $\hat{B}$ . The bare solid lines present analytical results of the approximation given by eqn (27) for  $\lambda_x, \lambda_y, \lambda_z$ . The dashed line in Fig. 4 shows the eigenvalue  $\lambda_0$  for the isotropic network (at  $H = 0$ ) as function of the parameter  $\theta$ .

First, it can be seen that application of the magnetic field leads to the splitting of the spectrum  $\lambda$  into two main branches for motions along the external magnetic field ( $\lambda_x$ ) and perpendicular to the field ( $\lambda_y, \lambda_z$ ). Moreover, the higher is the magnetic field, the higher is the splitting: the values  $\lambda_x$  ( $\lambda_x < \lambda_0$ ) decrease as a function of  $M/M^*$ , whereas  $\lambda_y = \lambda_z$  increase ( $\lambda_y, \lambda_z > \lambda_0$ ). This tendency can be explained by the fact that the inverse relaxation time  $\lambda_\alpha$  is proportional to the effective elasticity along the  $\alpha$ -axis. As we have shown, the effective elasticity along the  $x$ -axis decreases (eqn (9)) leading to the decrease of  $\lambda_x$ , whereas the elasticity along the  $y$ -axis increases (eqn (8)) leading to the increase of  $\lambda_y$ . Moreover, one can see from Fig. 4 that the discrepancies between the exact value  $\lambda_1, \lambda_2, \lambda_3$  and their approximation  $\lambda_x, \lambda_y, \lambda_z$  at equal values of  $\theta_x = \theta_y = \theta_z$  are negligible in the region  $M/M^* \leq 0.9$ .

In a general case  $\theta_x \neq \theta_y \neq \theta_z$  the values of  $\lambda_\alpha$  are different:  $\lambda_x \neq \lambda_y \neq \lambda_z$ . Fig. 5 shows relative deviations between the values  $\lambda_1, \lambda_2, \lambda_3$  and  $\lambda_x, \lambda_y, \lambda_z$  averaged over the vector  $\boldsymbol{\theta}$ , running in

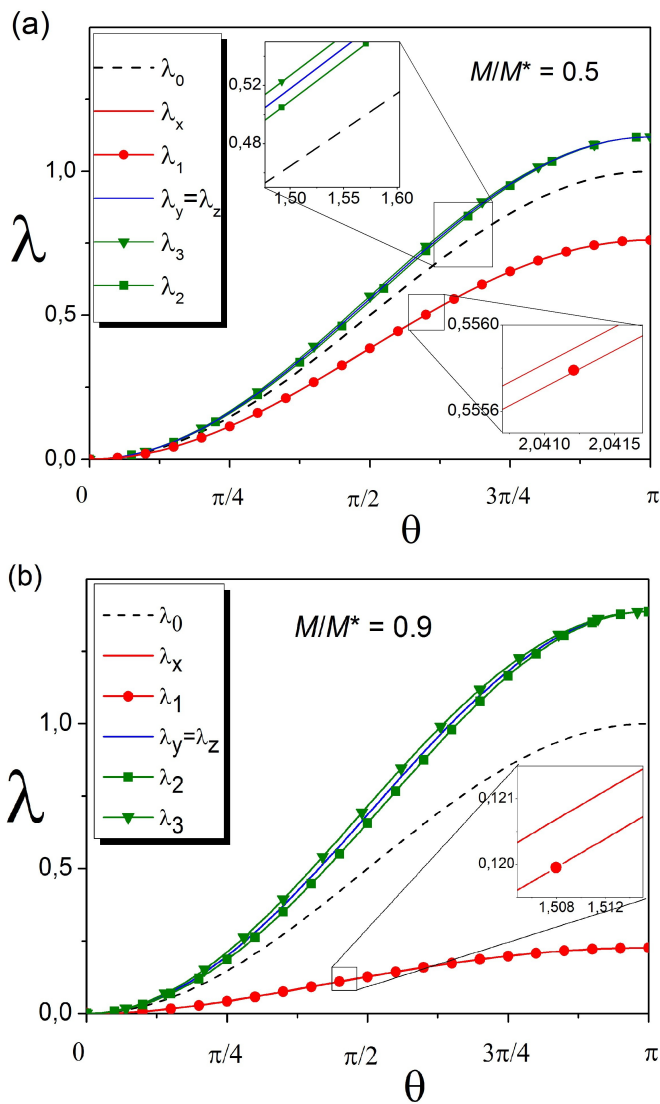


Fig. 4 Dependence of  $\lambda_0$ ,  $\lambda_x$ ,  $\lambda_y$ ,  $\lambda_z$  and  $\lambda_1$ ,  $\lambda_2$ ,  $\lambda_3$  on  $\theta = \theta_x = \theta_y = \theta_z$ .

a cube  $\theta_\alpha \in [0, \pi]$ ,  $\alpha = x, y, z$ :  $\varepsilon_1 = \langle \frac{|\lambda_1 - \lambda_x|}{\lambda_x} \rangle$ ,  $\varepsilon_2 = \langle \frac{|\lambda_2 - \min(\lambda_y, \lambda_z)|}{\min(\lambda_y, \lambda_z)} \rangle$  and  $\varepsilon_3 = \langle \frac{|\lambda_3 - \max(\lambda_y, \lambda_z)|}{\max(\lambda_y, \lambda_z)} \rangle$ . One can see from Fig. 5 that the values of the average deviations  $\varepsilon_{2,3}$  for the modes perpendicular to the external magnetic field are smaller than 0.5% for  $M \leq M^*$ . The value of the average deviation  $\varepsilon_1$  for the mode along the external magnetic field is smaller than 0.5% at  $M \leq 0.9M^*$  and then rapidly increases when  $M \rightarrow M^*$ , i.e., when  $M$  approaches to the boundary of the validity range of the model. Below we will perform calculations of the frequency dependent dynamic moduli in the range  $M \leq 0.9M^*$ , neglecting the non-diagonal terms of the matrix  $\hat{A}$  and approximating the eigenvalues by eqn (27).

#### 4 Dynamic moduli of MSE

For calculation of the dynamic moduli of MSEs we will use a formalism developed previously by one of the authors for anisotropic networks.<sup>35,52</sup> As in refs.<sup>35,52</sup> we consider infinitesimal periodic shear deformation,  $\gamma$ , applied along the  $\alpha$ -axis with the shear gradient along the  $\beta$ -axis (see Fig. 1). Orientation of the ex-

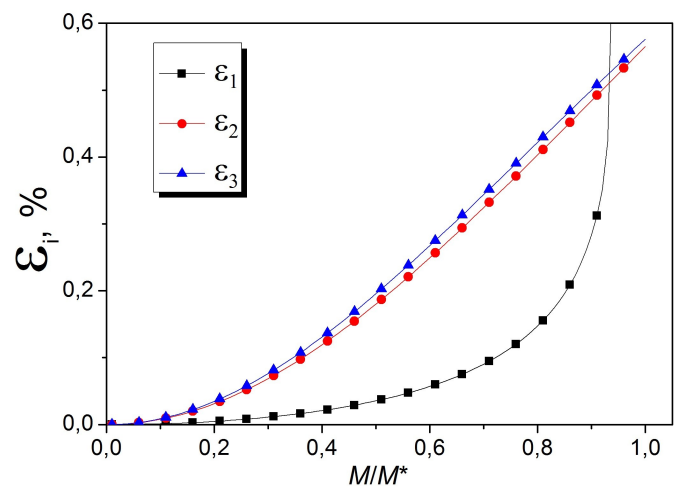


Fig. 5 Dependence of the average deviations  $\varepsilon_i$  ( $i = 1, 2, 3$ ) on  $M/M^*$ .

ternal magnetic field  $\mathbf{H}$  along three particular directions (the  $\alpha$ - and  $\beta$ -axis as well as perpendicular to the  $\alpha\beta$ -plane) reproduces three principal experimental geometries, denoted by  $\mathbf{G}$ ,  $\mathbf{V}$  and  $\mathbf{D}$  in Fig. 1.

The shear deformation results in appearance of the mechanical stress,  $\sigma_{\alpha\beta}$ . At small shear rates  $\dot{\gamma}(t)$  the shear stress depends linearly on  $\dot{\gamma}(t)$  and can be written in the following form:<sup>35,52,58</sup>

$$\sigma_{\alpha\beta}(t) = \int_{-\infty}^t dt' G_{\alpha\beta}(t-t') \dot{\gamma}(t'), \quad (28)$$

where  $G_{\alpha\beta}(t)$  is the shear relaxation modulus for a given  $\alpha\beta$ -geometry. Using assumption  $A_{\alpha\beta} = 0$  ( $\alpha \neq \beta$ ), the equation of motion (eqn (14)) for MSEs becomes similar to the equation of motion for anisotropic LC-networks.<sup>35</sup> Note that in spite of the difference between the physical phenomena, which are considered here and in ref.<sup>35</sup>, both of them can be described by the same mathematical formalism. Using the formalism developed in ref.<sup>35</sup> for the relaxation modulus of anisotropic networks, expression for  $G_{\alpha\beta}$  of an MSE can be written in our notation as follows:

$$G_{\alpha\beta}(t) = G_{\alpha\beta}^{(eq)} + \frac{k_B T}{V} \sum_{\mathbf{p}} \frac{\lambda_{\alpha,\mathbf{p}}}{\lambda_{\beta,\mathbf{p}}} e^{-(\tau_{\alpha,\mathbf{p}}^{-1} + \tau_{\beta,\mathbf{p}}^{-1})t}, \quad (29)$$

where  $G_{\alpha\beta}^{(eq)}$  is the equilibrium (static) shear modulus,  $k_B$  is the Boltzmann constant,  $T$  is the absolute temperature,  $V$  is the volume of the network, index  $\mathbf{p}$  numerates all normal modes in the 3D cubic network. Note, the equilibrium shear modulus  $G_{\alpha\beta}^{(eq)}$  for MSEs was considered in our recent work.<sup>17</sup>

For a finite network with fixed boundaries, the index  $\theta$  runs over the discrete values:

$$\theta_{\mathbf{p}} = \frac{\pi}{N_c} (p_x, p_y, p_z). \quad (30)$$

Here the integers  $p_\alpha$  run from 1 to  $N_c - 1$ , where  $N_c$  is the number of cells of the finite network along the  $x$ -,  $y$ - and  $z$ -axis. The total number of the cells is  $N_c^3$ . For the infinite network ( $N_c \rightarrow \infty$ ) the sum over indexes  $p_\alpha$  can be replaced by the integral over the

vector  $\boldsymbol{\theta}$  in the volume  $\Omega$  of the cube with the side length  $\pi$ :

$$\frac{1}{N_c^3} \sum_{p_x, p_y, p_z} \rightarrow \frac{1}{\pi^3} \int_{\Omega} d\boldsymbol{\theta} \quad (31)$$

and eqn (29) can be rewritten as follows:

$$G_{\alpha\beta}(t) = G_{\alpha\beta}^{(eq)} + ck_B T \frac{1}{\pi^3} \int_{\Omega} d\boldsymbol{\theta} \frac{\lambda_{\alpha}(\boldsymbol{\theta})}{\lambda_{\beta}(\boldsymbol{\theta})} e^{-(\lambda_{\alpha}(\boldsymbol{\theta}) + \lambda_{\beta}(\boldsymbol{\theta}))t/\tau_0}, \quad (32)$$

where  $c = N_c^3/V$  is the number of magnetic particles in the unit volume.

The dynamic shear modulus  $G_{\alpha\beta}^*(\omega)$  is related with the relaxation modulus  $G_{\alpha\beta}(t)$  as:

$$G_{\alpha\beta}^*(\omega) = i\omega \int_0^{\infty} G_{\alpha\beta}(t) e^{-i\omega t} dt, \quad (33)$$

where  $\omega = 2\pi f$  is the angular frequency. The real and imaginary parts of  $G_{\alpha\beta}^*$  give the storage and loss moduli:  $G'_{\alpha\beta} = \text{Re}(G_{\alpha\beta}^*)$  and  $G''_{\alpha\beta} = \text{Im}(G_{\alpha\beta}^*)$ . Substituting eqn (32) into (33) we obtain:

$$G'_{\alpha\beta}(\omega) = G_{\alpha\beta}^{(eq)} + ck_B T \frac{1}{\pi^3} \int_{\Omega} d\boldsymbol{\theta} \frac{\lambda_{\alpha}(\boldsymbol{\theta})}{\lambda_{\beta}(\boldsymbol{\theta})} \frac{(\omega\tau_0)^2}{[\lambda_{\alpha}(\boldsymbol{\theta}) + \lambda_{\beta}(\boldsymbol{\theta})]^2 + (\omega\tau_0)^2}, \quad (34)$$

$$G''_{\alpha\beta}(\omega) = ck_B T \frac{1}{\pi^3} \int_{\Omega} d\boldsymbol{\theta} \frac{\lambda_{\alpha}(\boldsymbol{\theta})}{\lambda_{\beta}(\boldsymbol{\theta})} \frac{\omega\tau_0(\lambda_{\alpha}(\boldsymbol{\theta}) + \lambda_{\beta}(\boldsymbol{\theta}))}{[\lambda_{\alpha}(\boldsymbol{\theta}) + \lambda_{\beta}(\boldsymbol{\theta})]^2 + (\omega\tau_0)^2}. \quad (35)$$

Varying the sets of the indices  $\alpha$  and  $\beta$ , we can calculate the moduli for the three principal geometries:  $(\alpha, \beta) = (y, x)$  for the **G**-geometry ( $G'_{yx} = G'_G$ ),  $(\alpha, \beta) = (y, z)$  for the **V**-geometry ( $G'_{yz} = G'_V$ ) and  $(\alpha, \beta) = (x, y)$  for the **D**-geometry ( $G'_{xy} = G'_D$ ). Fig. 6a, 6b, 6c show the frequency dependences of the storage (filled symbols) and loss (open symbols) moduli for **G**-, **V**- and **D**-geometries, respectively, at varying values of the reduced magnetisation  $M/M^*$ . The black lines in Fig. 6a, 6b, 6c illustrate the moduli for an isotropic network at the absence of the magnetic field. As can be seen from eqn (34)-(35),  $G'_G = G'_V = G'_D$  at  $H = 0$  and the dynamic moduli  $G_{\alpha\beta}^*$  coincide with the dynamic modulus for the isotropic network found in ref. 35,37,38

The coarse-grained cubic model provides the asymptotic power-law of the storage modulus with the exponent 3/2: 35-38  $(G' - G^{(eq)})/ck_B T \sim \omega^{3/2}$  at  $\omega < \tau_0^{-1}$ , as can be seen from Fig. 6. This feature distinguishes the cubic network model from, e.g., Maxwell model, which predicts the asymptotic power-law behavior with the exponent 2:  $(G' - G^{(eq)})/ck_B T \sim \omega^2$  at  $\omega < \tau_M^{-1}$ , where  $\tau_M$  is the single time in the Maxwell model. The frequency behavior  $\sim \omega^{3/2}$  of storage modulus of the polymer networks is caused by the contribution not only from a single mode of motion but by the set of all collective modes from chains included into the united network structure.

Note that since we consider only the long-scale modes at  $\tau > \tau_0$ , the density  $c$  in eqn (32)-(35) determines the concentration of the magnetic particles in MSE sample. However, after including all the nano-scale modes at  $\tau < \tau_0$ , the density  $c$  in the prefactor will become the density of the Kuhn segments. 43 In this case, even the absolute value  $ck_B T$  will be in the quantitative agreement with characteristic experimental values of the moduli:  $ck_B T \sim 10^5 - 10^6$  Pa. 43 However, contribution of the nano-scale modes to the dy-

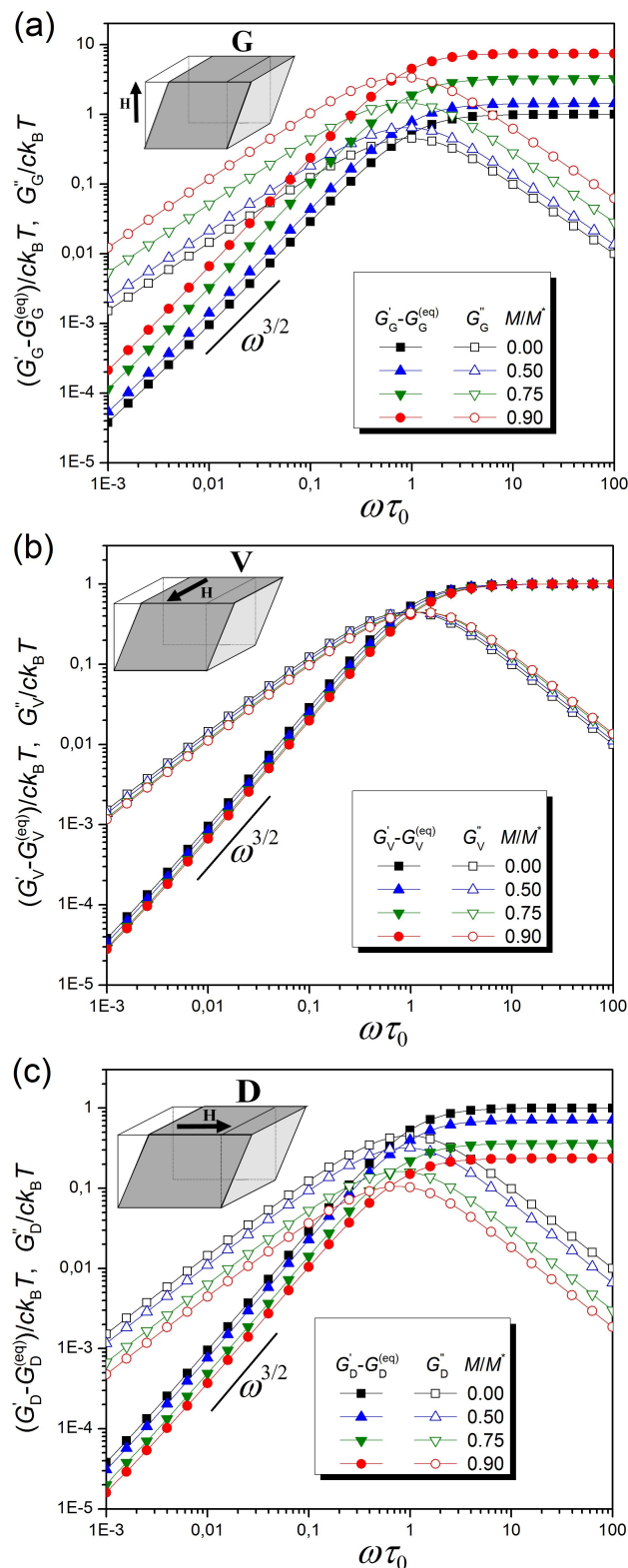


**Fig. 6** Reduced storage  $G'$  and loss  $G''$  moduli as functions of the reduced frequency  $\omega\tau_0$  for the **G**-, **V**-, **D**-geometries, calculated at  $M/M^* = 0.00, 0.50, 0.75, 0.90$ ;  $\tau_0$  is the minimal relaxation time of the cubic network at the absence of the magnetic field.

dynamic moduli of MSE is the special task. Since our model includes only long-scale modes at  $\tau > \tau_0$ , presently it makes sense to com-

pare the relative changes of the moduli with respect to the initial values, but not the absolute values.

The blue, green and red lines in Fig. 6a, 6b, 6c show the moduli of MSEs at the presence of the magnetic field with  $M/M^* = 0.50, 0.75, 0.90$ , respectively, as compared to the initial values at  $M = 0$  (black lines). One can see that application of the external magnetic field leads to the different behaviour of the dynamic moduli of MSEs for different geometries. The modulus  $G_G^*$  increases and  $G_D^*$  decreases significantly, whereas  $G_V^*$  changes slightly with increase of the magnetic field. This tendency can be explained by the fact that the moduli are proportional to the different combinations of the inverse relaxation times:  $G_G^* \propto \lambda_y/\lambda_x$ ,  $G_V^* \propto \lambda_y/\lambda_z \approx 1$  and  $G_D^* \propto \lambda_x/\lambda_y$ . As we have shown above (see Fig. 4), the inverse relaxation time  $\lambda_x$  decreases, whereas the inverse relaxation times  $\lambda_y$  and  $\lambda_z$  increase with increase of the magnetic field. This leads to the increase of  $G_G^*$  and to the decrease of  $G_D^*$ . At the same time, the difference between  $\lambda_y$  and  $\lambda_z$  is sufficiently small and, thus, the dynamic modulus  $G_V^*$  changes only slightly with increase of the magnetic field.

It is important to point out that our model predicts the values of the dynamic moduli for the G-geometry, which are in a qualitative agreement with experimental data. Many experimental works demonstrate that both  $G_G'$  and  $G_G''$  increase with increase of the magnetic field and the change of their values at fixed frequency can reach up to 1 or even 2 decades at experimentally investigated magnetic flux densities.<sup>6,25,27,29,50</sup> As can be seen from Fig. 6a, the proposed model provides the change of  $G_G'$  and  $G_G''$  up to one decade at  $B < B^*$ . The V- and D-geometries were not yet studied in experiments. Thus, the theoretical results for these geometries can be considered as a prediction of the theory.

## 5 Comparison with experimental data. Discussion

In this section we will demonstrate that the theoretical formalism proposed above allows to analyze the experimental data for the G-geometry also quantitatively. Since eqn (34)-(35) for the dynamic moduli include a numerical integration, we use an additional approximation for the inverse relaxation times to simplify the calculations. As we discussed above, the values of  $\lambda_x$  and  $\lambda_y$  are proportional to the effective elasticity constants for motions along  $x$ - and  $y$ -axis. According to eqn (8)-(9) these elasticity constants can be introduced as:

$$K_x^{(\text{eff})} = K \left[ 1 - (M/M^*)^2 \right], \quad (36)$$

$$K_y^{(\text{eff})} = K \left[ 1 + 0.5(M/M^*)^2 \right]. \quad (37)$$

Thus, the ratio between  $\lambda_x$  and  $\lambda_y$  can be approximated by the ratio between appropriate elasticity constants:

$$\frac{\lambda_y}{\lambda_x} \cong \frac{1 + 0.5(M/M^*)^2}{1 - (M/M^*)^2}. \quad (38)$$

In this approach, the ratio  $\lambda_y/\lambda_x$  in eqn (34)-(35) for the G-geometry is independent of the integration variable  $\theta$  and can be taken out of the integrals. Using the approximation  $\lambda_x \approx \lambda_y \approx \lambda_0$  in the integrands, the remaining integrals with the prefactor

$ck_B T/\pi^3$  are equal to the storage  $G_0'(\omega)$  and loss  $G_0''(\omega)$  moduli at the absence of the magnetic field:  $G_0'(\omega) = G'(\omega)|_{H=0}$  and  $G_0''(\omega) = G''(\omega)|_{H=0}$ . At small  $M/M^*$  we obtain the following approximate equations:

$$G' \simeq G_0 \left[ 1 + 1.2(M/M^*)^2 \right] + (G_0' - G_0) \left[ 1 + 1.5(M/M^*)^2 \right], \quad (39)$$

$$G'' \simeq G_0'' \left[ 1 + 1.5(M/M^*)^2 \right], \quad (40)$$

where  $G_0$  is the static shear modulus at the absence of the magnetic field given by eqn (2). Here we used a prediction for the equilibrium shear modulus  $G_G^{(\text{eq})}$ , obtained in the framework of the cubic lattice model:<sup>17</sup>  $G_G^{(\text{eq})} \simeq G_0 \left[ 1 + 1.2(M/M^*)^2 \right]$ . Using an identity of the ratios  $M/M^*$  and  $B/B^*$ , eqn (39)-(40) can be rewritten as follows:

$$G' \simeq G_0' + C_1 B^2, \quad (41)$$

$$G'' \simeq G_0'' + C_2 B^2, \quad (42)$$

where the frequency-dependent coefficients  $C_1$  and  $C_2$  are determined by the structural parameters of the model  $B^*$ ,  $G_0'$ ,  $G_0''$  and  $G_0$ , as it follows from eqn (39)-(42):

$$C_1 = \frac{1.5}{(B^*)^2} (G_0' - 0.2G_0), \quad (43)$$

$$C_2 = \frac{1.5}{(B^*)^2} G_0''. \quad (44)$$

Here we recall that the critical value  $B^*$  depends on the volume fraction of magnetic particles and on the static modulus of the composite according to eqn (11). Thus, eqn (41)-(44) provide explicitly the structure-property relationships for the dynamic moduli for MSEs using a microscopic dynamic model.

Now, we use eqn (41) and (42) to analyse experimental data for  $G'$  and  $G''$  measured at a constant frequency. As an example, we consider the experimental data of ref.<sup>26</sup> for the storage and loss moduli, measured as functions of the magnetic field  $B$  in the range  $B = 0..700$  mT at  $f = 10$  Hz and for different volume fractions  $\phi$ . For our theoretical analysis we use the data for  $G'$  and  $G''$  at low magnetic field ( $B = 0..200$  mT), shown in Fig. 7 by solid lines with the symbols. This regime corresponds to the validity range of our model.

The fits are shown by the dashed lines in Fig. 7 and the fitting parameters  $G_0'$ ,  $C_1$ ,  $G_0''$  and  $C_2$  are presented in Table 1. The experimentally measured volume fractions  $\phi$  are given in the first column. Parameters  $G_0'$ ,  $C_1$ ,  $G_0''$  and  $C_2$  allow us to estimate the structural parameters  $B^*$  and  $G_0$  using eqn (43)-(44):

$$B^* = \left( \frac{1.5G_0''}{C_2} \right)^{1/2}, \quad (45)$$

$$G_0 = 5 \left( G_0' - \frac{C_1 G_0''}{C_2} \right). \quad (46)$$

Finally, using the values of  $B^*$  and  $G_0$  we estimate theoretically

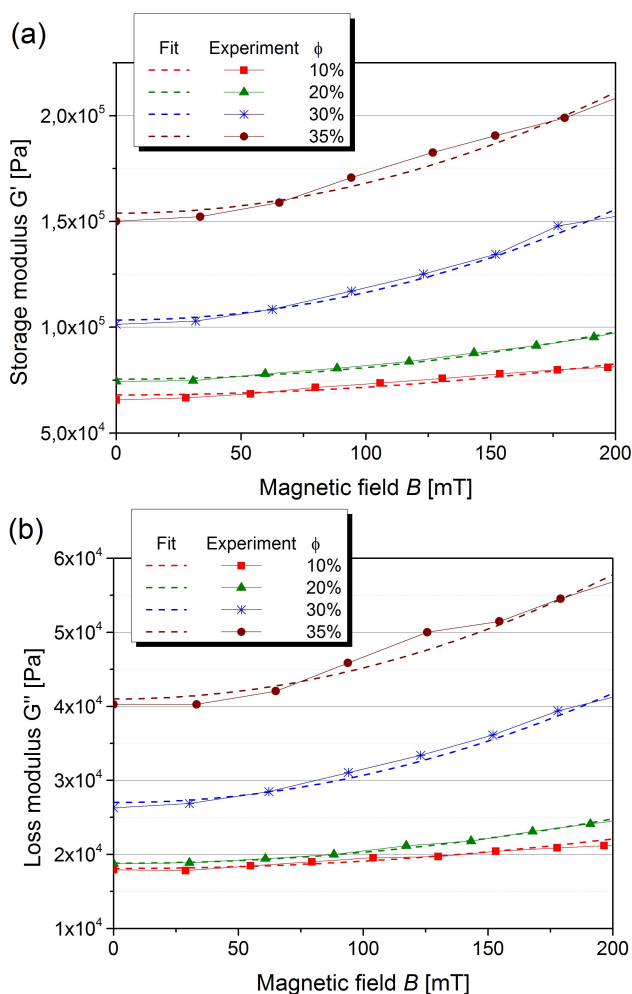


**Fig. 7** Dependences of  $G'$  (a) and  $G''$  (b) on the magnetic flux density  $B$  at  $f = 10$  Hz and at different volume fraction  $\phi = 10\%$ ,  $20\%$ ,  $30\%$  and  $35\%$ . Solid lines with the symbols illustrate the experimental data extracted from ref.,<sup>26</sup> dashed lines show their fitting according to eqn (41)-(42).

the volume fraction  $\phi_{th}$  according to eqn (11):

$$\phi_{th} = \left( \frac{4\pi\mu_0 G_0}{63(B^*)^2} \right)^{1/2}. \quad (47)$$

The values of  $B^*$ ,  $G_0$  and  $\phi_{th}$  estimated for each experimental volume fraction  $\phi$  are shown in Table 1.

From this table one can see that the static shear modulus  $G_0$  increases with increase of the volume fraction. It is approximately 2-7 times smaller than the storage modulus  $G'_0$  measured at 10 Hz and at the absence of the external magnetic field. Here we note that the static modulus  $G_0 = G'_0(\omega \rightarrow 0)$  can be up to one order of magnitude smaller than  $G'_0$  measured at 10 Hz.<sup>25,29,43</sup> Additionally, we obtain the values of  $\phi_{th}$ , which are very close to the experimental values  $\phi$ . This good agreement of the theoretical results with experimental data demonstrates a great potential strength of the proposed theoretical formalism to study the dynamic properties of MSEs of different structures. The formalism can be considered as a basis for future studies of the ef-

**Table 1** Fitting parameters  $G'_0$ ,  $C_1$ ,  $G''_0$ ,  $C_2$  and estimated values of  $B^*$ ,  $G_0$  and  $\phi_{th}$ .

$\phi$ , %	$G'_0$ , [kPa]	$C_1$ , $[\frac{\text{Pa}}{(\text{mT})^2}]$	$G''_0$ , [kPa]	$C_2$ , $[\frac{\text{Pa}}{(\text{mT})^2}]$	$B^*$ , [mT]	$G_0$ , [kPa]	$\phi_{th}$ , %
10	68.0	0.37	17.9	0.10	518	8.9	9.1
20	75.4	0.56	18.8	0.15	434	26.1	18.6
30	103.4	1.31	27.0	0.37	331	39.0	29.9
35	153.9	1.43	41.0	0.42	383	71.5	35.0

fects of complex network structure (such as short-scale segmental motions inside the network strand, heterogeneous distribution of cross-links, polydispersity of network strands, the presence of dangling chains and loops, etc.) on the dynamic properties of MSEs. Especially, the influence of particle distribution on the dynamic moduli of MSEs can be a topic of further theoretical developments, for example, based on hexagonal or body-centered cubic network models, which were used to study the static moduli of MSEs.<sup>18,57</sup>

## 6 Conclusions

A viscoelastic microscopic model has been introduced for description of the low-frequency dynamics of magneto-sensitive elastomers with isotropically distributed magnetic particles under external homogeneous magnetic field. The network domains between neighbouring particles are represented in the low-frequency regime by linear Hookean springs, which connect the near-neighbour particles. Equations of motions take into account the influence of mechanical and magnetic forces on the dynamics of magnetic particles. The theory is developed for magnetic flux densities below the critical value  $B^*$ , at which the magnetic particles are only able to fluctuate around their average positions and do not rearrange into chain-like clusters under the magnetic field. The critical value  $B^*$  increases as a function of the elastic modulus of the composite. The range  $B < B^*$  corresponds to experimentally studied ranges of the magnetic fields:  $B^* \sim 200 - 800$  mT.

The relaxation spectrum and the frequency-dependent shear moduli  $G'$  and  $G''$  of MSEs are calculated as functions of the magnetic field. We show that application of the external magnetic field can lead to the increase or decrease of  $G'$  and  $G''$  depending on a mutual arrangement of the magnetic field vector and the direction of shear deformation. Three principal geometries of shear deformation are considered, in which the magnetic field  $\mathbf{H}$  is applied along the shear gradient vector (**G**-geometry), along the shear displacement vector (**D**-geometry) and perpendicular to the plane formed by these two vectors (**V**-geometry).

In the **G**-geometry the value of  $G'_G$  increases with increase of the magnetic field and can reach up to one order of magnitude. This result of our theory agrees well with experimental studies.<sup>6,25,27,29,50</sup> Further, we show that in the **V**-geometry the shear deformation is disturbed only slightly by the presence of the external magnetic field. An opposite picture is found for the **D**-geometry, where application of the external magnetic field softens the magnetised sample considerably. The results for the shear moduli in the **D**- and **V**-geometries can be considered as predictions of the theory. Moreover, we propose a simple fitting proce-

ture, which allows to describe experimental data and to extract a number of structural characteristics of MSEs. The extracted values of the volume fraction are close to experimental ones and the calculated static shear moduli of MSEs have a reasonable magnitude.

The frequency dependences of the dynamic moduli show tendencies in a qualitative agreement with a number of experimental data: the moduli are increasing functions of frequency in the low-frequency regime.<sup>6,25,27,29,50</sup> However, the exponents  $\alpha$  and  $\beta$  of the frequency dependences  $G' \propto \omega^\alpha$  and  $G'' \propto \omega^\beta$  are expected to be very sensitive to the connectivity of network strands. The dependence of the exponents  $\alpha$  and  $\beta$  on the network structure demands a special analysis as it was shown in a number of theoretical works for non-magnetic polymer networks.<sup>36–45</sup> The similar analysis for MSEs can be a topic of further theoretical investigations.

We hope that our theoretical findings will initiate new experimental studies of the dynamic mechanical properties of MSEs for different geometries of the magnetic field with respect to the oscillating mechanical loading.

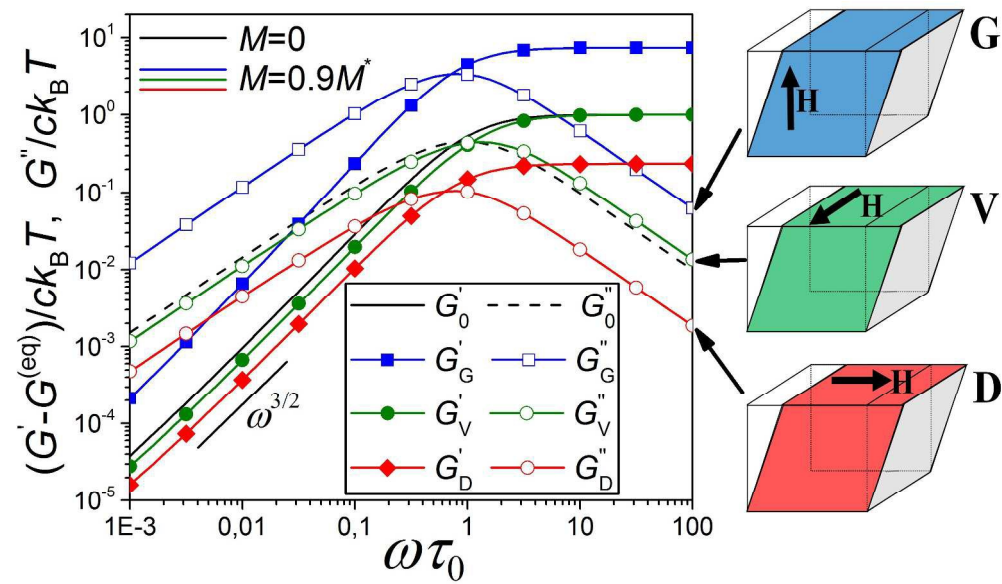
## Acknowledgement

The financial support of the DFG grant GR 3725/6-1 is gratefully acknowledged.

## References

- O. V. Stolbov, Y. L. Raikher and M. Balasoiu, *Soft Matter*, 2011, **7**, 8484–8487.
- D. J. Carlson and M. R. Jolly, *Mechatronics*, 2000, **10**, 555–569.
- W. Li and X. Zhang, *Recent Patents on Mechanical Engineering*, 2008, **1**, 161–166.
- C. Bellan and G. Bossis, *International Journal of Modern Physics B*, 2002, **16**, 2447–2453.
- J. L. Arias, V. Gallardo, F. Linares-Molinero and A. V. Delgado, *Journal of Colloid and Interface Science*, 2006, **299**, 599–607.
- A. Boczkowska and S. F. Awietjan, *Journal of Materials Science*, 2009, **44**, 4104–4111.
- M. Lokander and B. Stenberg, *Polymer Testing*, 2003, **22**, 677–680.
- D. Borin, D. Günther, C. Hintze, G. Heinrich and S. Odenbach, *Journal of Magnetism and Magnetic Materials*, 2012, **324**, 3452–3454.
- E. Coquelle and G. Bossis, *Journal of Advanced Science*, 2005, **17**, 132–138.
- G. Diguët, E. Beaugnon and J. Y. Cavallé, *Journal of Magnetism and Magnetic Materials*, 2010, **322**, 3337–3341.
- G. Filipcsei and M. Zrinyi, *Journal of Physics: Condensed Matter*, 2010, **22**, 276001.
- D. Y. Borin, G. V. Stepanov and S. Odenbach, *Journal of Physics: Conference Series*, 2013, **412**, 012040.
- M. R. Jolly, J. D. Carlson, B. C. Muñoz and T. A. Bullions, *Journal of Intelligent Material Systems and Structures*, 1996, **7**, 613–622.
- L. C. Davis, *Journal of Applied Physics*, 1999, **85**, 3348–3351.
- Y. L. Raikher and O. V. Stolbov, *Technical Physics Letters*, 2000, **26**, 156–158.
- T. Taniguchi, T. Mitsumata, M. Sugimoto and K. Koyama, *Physica A: Statistical Mechanics and its Applications*, 2006, **370**, 240–244.
- D. Ivaneyko, V. P. Toshchevikov, M. Saphiannikova and G. Heinrich, *Macromolecular Theory and Simulations*, 2011, **20**, 411–424.
- D. Ivaneyko, V. Toshchevikov, M. Saphiannikova and G. Heinrich, *Condensed Matter Physics*, 2012, **15**, 33601.
- Y. Han, W. Hong and L. E. Faidley, *International Journal of Solids and Structures*, 2013, **50**, 2281–2288.
- G. Pessot, P. Cremer, D. Y. Borin, S. Odenbach, H. Löwen and A. M. Menzel, *The Journal of Chemical Physics*, 2014, **141**, 124904.
- G. V. Stepanov, D. Y. Borin, Y. L. Raikher, P. V. Melenev and N. S. Perov, *Journal of Physics: Condensed Matter*, 2008, **20**, 204121.
- R. Weeber, S. Kantorovich and C. Holm, *Soft Matter*, 2012, **8**, 9923–9932.
- L. Chen, X. Gong and W. Li, *Chinese Journal of Chemical Physics*, 2008, **21**, 581–585.
- D. Y. Borin and G. V. Stepanov, *Journal of Optoelectronics and Advanced Materials*, 2013, **15**, 249–253.
- H. Böse, *International Journal of Modern Physics B*, 2007, **21**, 4790–4797.
- H. Böse and R. Röder, *Journal of Physics: Conference Series*, 2009, **149**, 012090.
- A. V. Chertovich, G. V. Stepanov, E. Y. Kramarenko and A. R. Khokhlov, *Macromolecular Materials and Engineering*, 2010, **295**, 336–341.
- C. Karl, J. McIntyre, T. Alshuth and M. Klüppel, *Kautschuk Gummi Kunststoffe*, 2013, **1–2**, 46–53.
- V. V. Sorokin, E. Ecker, G. V. Stepanov, M. Shamonin, G. J. Monkman, E. Y. Kramarenko and A. R. Khokhlov, *Soft Matter*, 2014, **10**, 8765–8776.
- S. Aloui and M. Klüppel, *Smart Materials and Structures*, 2015, **24**, 025016.
- N. Hoang, N. Zhang and D. H., *Smart Materials and Structures*, 2009, **18**, 074009.
- N. Hoang, N. Zhang and D. H., *Smart Materials and Structures*, 2011, **20**, 015019.
- L. Chen and S. Jerrams, *Journal of Applied Physics*, 2011, **110**, 013513.
- M. Tarama, P. Cremer, D. Y. Borin, S. Odenbach, H. Löwen and A. M. Menzel, *Physical Review E*, 2014, **90**, 042311.
- V. P. Toshchevikov and Y. Y. Gotlib, *Macromolecules*, 2009, **42**, 3417–3429.
- Y. Y. Gotlib, *Pure & Appl. Chem.*, 1981, **53**, 1531–1540.
- A. A. Gurtovenko and Y. Y. Gotlib, *Macromolecules*, 2000, **33**, 6578–6587.
- A. A. Gurtovenko and A. Blumen, *Advances in Polymer Science*, 2005, **182**, 171–282.
- A. A. Gurtovenko, Y. Y. Gotlib and H.-G. Kilian, *Macromolecu-*

- lar Theory and Simulations, 2000, **9**, 388–397.
- 40 J.-U. Sommer, *The Journal of Chemical Physics*, 1991, **95**, 1316–1317.
- 41 J. G. Curro and P. Pincus, *Macromolecules*, 1983, **16**, 559–562.
- 42 K. Schwenke, M. Lang and J.-U. Sommer, *Macromolecules*, 2011, **44**, 9464–9472.
- 43 M. Saphiannikova, V. Toshchevnikov, I. Gazuz, F. Petry, S. Westermann and G. Heinrich, *Macromolecules*, 2014, **47**, 4813–4823.
- 44 A. Jurjiu, C. Friedrich and A. Blumen, *Chemical Physics*, 2002, **284**, 221–231.
- 45 F. Fürstenberg, M. Dolgushev and A. Blumen, *The Journal of Chemical Physics*, 2013, **138**, 034904.
- 46 V. P. Toshchevnikov and Y. Y. Gotlib, *Polymer Science, Series A*, 2006, **48**, 649–663.
- 47 V. P. Toshchevnikov, A. Blumen and Y. Y. Gotlib, *Macromolecular Theory and Simulations*, 2007, **16**, 359–377.
- 48 V. P. Toshchevnikov, M. Saphiannikova and G. Heinrich, *The Journal of Chemical Physics*, 2012, **137**, 024903.
- 49 V. Toshchevnikov and Y. Y. Gotlib, *Polymer Science Series A*, 2013, **55**, 556–56.
- 50 G. V. Stepanov, S. S. Abramchuk, D. A. Grishin, L. V. Nikitin, E. Y. Kramarenko and A. R. Khokhlov, *Polymer*, 2007, **48**, 488–495.
- 51 C. Hintze, D. Y. Borin, D. Ivaneyko, V. Toshchevnikov, M. Saphiannikova-Grenzer and G. Heinrich, *Kautschuk Gummi Kunststoffe*, 2014, **4**, 53–59.
- 52 V. P. Toshchevnikov, G. Heinrich and Y. Y. Gotlib, *Macromolecular Theory and Simulations*, 2010, **19**, 195–209.
- 53 Y. L. Raikher and O. V. Stolbov, *Journal of Physics: Condensed Matter*, 2008, **20**, 204126.
- 54 A. M. Biller, O. V. Stolbov and Y. L. Raikher, *Journal of Applied Physics*, 2014, **116**, 114904.
- 55 X. Guan, X. Dong and J. Ou, *Journal of Magnetism and Magnetic Materials*, 2008, **320**, 158–163.
- 56 G. Filipcsei, I. Csetneki, A. Szilágyi and M. Zrínyi, *Advances in Polymer Science*, 2007, **206**, 137–189.
- 57 D. Ivaneyko, V. Toshchevnikov, M. Saphiannikova and G. Heinrich, *Soft Matter*, 2014, **10**, 2213–2225.
- 58 M. Doi and S. F. Edwards, *The theory of polymer dynamic*, Clarendon Press – Oxford, 1986, p. 391.
- 59 J. D. Ferry, *Viscoelastic Properties of Polymers*, Wiley–VCH, 1980, p. 672.
- 60 M. Rubinstein and R. H. Colby, *Polymer Physics (Chemistry)*, Oxford University Press, USA, 2003, p. 454.



267x157mm (300 x 300 DPI)